Progress In Electromagnetics Research B, Vol. 60, 111–123, 2014

Design of Asymmetric Slot Antenna with Meandered Narrow Rectangular Slit for Dual Band Applications

Raj Kumar[1, *], Praveen V. Naidu[2], and Vivek Kamble[3]

Abstract—A compact, coplanar waveguide (CPW) fed asymmetric slot antenna with dual operating bands is proposed. The slot is modified rectangular in shape and asymmetrically cut in the ground plane. A hexagonal patch fed by a two-step CPW is used to excite the slot. The feed itself is slightly asymmetric (shifted, with unequal ground planes). The asymmetric cuts on the slot together with the feed line asymmetry have helped in obtaining ultra wideband impedance matching. An extra resonance at 2.4 GHz for Bluetooth applications is obtained by cutting an additional meandered narrow rectangular shape slit in the ground plane. The prototype of the proposed antenna has been fabricated and tested. The measured 10 dB return loss bandwidth of the proposed antenna is 200 MHz (2.3–2.5 GHz) for the first band and 12.1 GHz (2.9–15.0 GHz) for the second band. The radiation patterns of the proposed antenna are obtained and found to be Omni-directional in H-plane and bi-directional in E-plane. The measured and simulated results are in good agreement.

1. INTRODUCTION

In the year 2002, the Federal Communications Commission (FCC) released an unlicensed ultra wide band (UWB) frequency spectrum from 3.1 to 10.6 GHz for commercial communication applications [1]. UWB is a short distance radio communication technology which haves many advantages, such as wider bandwidth, low power output and high data rate (more than 100 Mbps) compared with traditional communication systems. Because of these advantages, a lot of interest has been generated in researchers and engineers for the development of UWB antennas for short-range wireless, imaging radar and remote sensing applications. Nowadays, several communication devices require the integration of more than one license-free communication standard into a single system due to the limited space available in the device [2]. Hence antennas are required to be cost effective, capable of operating in multiple frequency bands and easily integrated with other RF (radio frequency) circuits. Besides the UWB (3.1–10.6 GHz), other license free bands include the Bluetooth (2.40–2.484 GHz), Wireless broadband (WiBro) for broadband wireless internet (2.3–2.39 GHz) and IEEE 802.11b/g wireless local area network (WLAN).

Many UWB [3, 4] and dual-band [5–20] antennas have been reported in the open literature. In [5], a $30 \times 35\,\text{mm}^2$ dual-band antenna having a U-shaped open stub is proposed. The applications covered are the 2.45 GHz WLAN and the 3.1–5.2 GHz DS-UWB. In [6], a printed circular monopole with an annular slot and fed by microstrip line is used to cover the UWB and Bluetooth bands; the antenna dimension being $45 \times 32\,\text{mm}^2$. In [7], a $42 \times 46\,\text{mm}^2$, dual-band antenna is proposed. At the corner of a monopole antenna, an L-shaped resonant element is added to obtain the 2.4 GHz Bluetooth band in addition to the UWB (3.1–10.6 GHz). A $46 \times 55\,\text{mm}^2$ printed volcano smoke shape antenna for UWB and WLAN applications is presented in [8]. In [9], a compact $18 \times 32\,\text{mm}^2$ Bluetooth integrated UWB

Received 22 April 2014, Accepted 10 June 2014, Scheduled 17 June 2014

* Corresponding author: Raj Kumar (dr.rajkumarkumar@yahoo.com).

[1] ARDE, Pashan, Pune 411021, India. [2] Symbiosis International University, Pune, India. [3] DIAT (DU), Girinagar, Pune 411025, India.

antenna is proposed, however the return loss characteristic in the 2.4 GHz band appears distorted and shifted to higher frequency side. In [10–12], a printed fork-shaped patch is employed to realize dual-band characteristics for Bluetooth and UWB applications. In [13], a $40 \times 32\,\text{mm}^2$ open slot loaded monopole antenna is presented for 2.4–2.5 GHz WLAN and 3–10.6 GHz UWB applications. In [14], a two stepped microstrip feed is used to excite two narrow rectangular slots of different dimensions and placed parallel to each other. The antenna has a size of $60 \times 60\,\text{mm}^2$ and has operating bands from 2.25–2.53 GHz and 5.13–5.99 GHz. In [15], a $40 \times 40\,\text{mm}^2$ dual-band slot antenna consisting of a square ring slot and a circular ring slot is proposed. The design presented in [16] is a microstrip fed rectangular slot antenna for WLAN applications. The antenna further has a U-shaped metallic strip placed hanging inside the slot. Dual operating bands from 2.4–2.484 GHz and 5.150–5.950 GHz are obtained but with dimension of $75 \times 75\,\text{mm}^2$, the antenna is not quite portable for wireless communication devices. The various antennas are compared in Table 1. In comparison to these antennas, the proposed antenna is quite compact ($34 \times 30\,\text{mm}^2$), has a wider bandwidth, acceptable radiation patterns in the E and H-planes and a maximum peak gain of about 6 dBi. Moreover, it is excited using a CPW feed which makes it to be easily integrated with other RF circuits.

Table 1. Comparisons of antenna size of proposed antenna with other antennas.

S. No	Reference	Antenna Size	Measured Bandwidth
1.	Ref. [3]	$120 \times 100\,\text{mm}^2$	3.1–10.6 GHz
2.	Ref. [4]	$70 \times 70\,\text{mm}^2$	3.1–10.6 GHz
3.	Ref. [5]	$30 \times 35\,\text{mm}^2$	3.1–5.2 GHz
4.	Ref. [6]	$45 \times 32\,\text{mm}^2$	2.4–2.5 GHz and 3.1–10.6 GHz
5.	Ref. [7]	$42 \times 46\,\text{mm}^2$	2.4–2.484 GHz and 3.1–10.6 GHz
6.	Ref. [8]	$46 \times 55\,\text{mm}^2$	1.8–14.35 GHz
7.	Ref. [9]	$18 \times 32\,\text{mm}^2$	2.470–2.520 GHz and 3.1–10.6 GHz
8.	Ref. [10]	$50 \times 24\,\text{mm}^2$	2.4–2.484 GHz, 3.1–5.15 GHz and 5.825–10.6 GHz
9.	Ref. [11]	$42 \times 24\,\text{mm}^2$	2.4–2.484 GHz and 3.1–10.6 GHz
10.	Ref. [12]	$40 \times 32\,\text{mm}^2$	2.4–2.484 GHz and 3.1–10.6 GHz
11.	Ref. [13]	$60 \times 60\,\text{mm}^2$	2.25–2.53 GHz and 5.13–5.99 GHz
12.	Ref. [14]	$40 \times 40\,\text{mm}^2$	2.4–2.485 GHz and 5.15–5.825 GHz
13.	Ref. [15]	$75 \times 75\,\text{mm}^2$	2.4–2.484 GHz and 5.150–5.950 GHz
14.	Ref. [16]	$40 \times 40\,\text{mm}^2$	3.15–3.70 GHz and 5.05–5.97 GHz
15.	Ref. [17]	$60 \times 45\,\text{mm}^2$	2.26–2.57 GHz and 4.81–6.56 GHz
16.	Ref. [18]	$50 \times 50\,\text{mm}^2$	1.9–2.75 GHz and 3.65–6.75 GHz
17.	Ref. [19]	$60 \times 70\,\text{mm}^2$	3.34–3.54 GHz and 4.90–6.26 GHz
18.	Ref. [20]	$50 \times 50\,\text{mm}^2$	2384–2991 MHz and 4959–6410 MHz
19.	Proposed antenna	$34 \times 30\,\text{mm}^2$	2.3-2.5 GHz and 2.9-15.0 GHz

The proposed dual-band antenna has target frequency bands of 2.4–2.484 GHz (for Bluetooth application) and 3.1–10.6 GHz (for UWB applications). The antenna is composed of a modified chamfered rectangular shaped slot and a hexagonal patch fed by a two-step CPW. Asymmetric cuts are placed on the slot which together with the feed line asymmetry helps in obtaining ultra wideband impedance matching. For realizing another resonant band for Bluetooth application (near 2.4 GHz) without disturbing the UWB performance, a slot stub of suitable length is introduced in the ground plane. In the following sections, the antenna geometry is described, measured and simulated results are presented and the effects of antenna's key structural parameters on the performance are analyzed by means of a parametric study.

2. ANTENNA DESIGN

The geometry of the proposed CPW-fed dual-band antenna is given in Figure 1. The antenna has an overall dimension of $34 \times 30\,\text{mm}^2$ and is designed on a 1.58 mm thick FR4 substrate having relative permittivity of 4.4. The antenna consists of a hexagonal radiating patch, a two stepped CPW feed, a modified extended rectangular slot and a meandered rectangular slit in the ground plane. The feed is shifted towards the right side which makes the two halves of the ground plane unequal in size and introduces asymmetry in the design. The slot structure is initially taken rectangular and then changed step by step by observing the reflection coefficient characteristic for improvement in impedance matching. In the final stage, the design has a rectangular extension of size $L_8 \times W_6$ on one side and two of its corners are chamfered. To introduce an extra resonant frequency at 2.4 GHz for Bluetooth application without changing the UWB characteristics, a narrow meandered rectangular slit is cut in the ground plane. The width of the meandered slit is taken as 0.5 mm. All the parameters shown in Figure 1 have their dimensions given in Table 1.

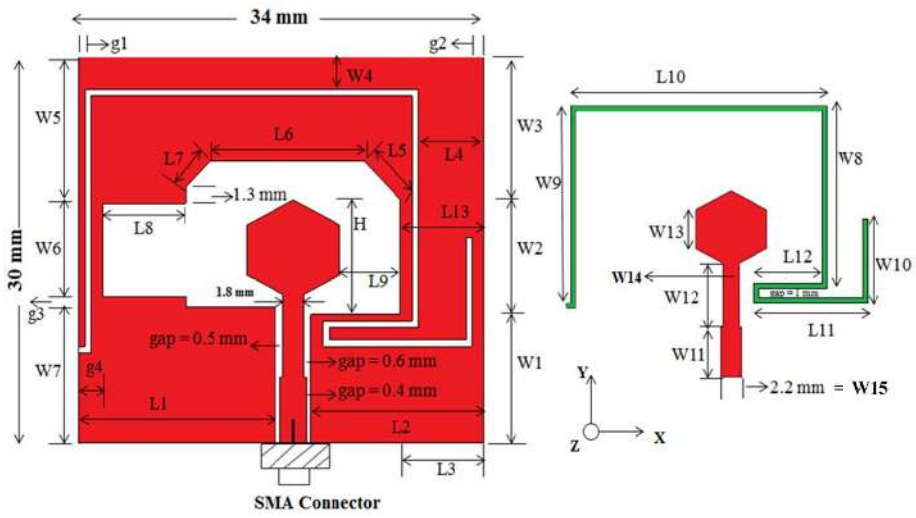

Figure 1. Geometry of the proposed antenna.

Table 2. Dimensions of parameters of the proposed antenna.

Parameter	W_1	W_2	W_3	W_4	W_5	W_6	W_7	g_1	g_4	W_{14}	W_{15}
Value (mm)	10	8.9	11.1	2.5	11.4	7.2	10.6	0.5	2	1.8	2.2
Parameter	W_8	W_9	W_{10}	W_{11}	W_{12}	W_{13}	L_1	L_2	L_3	g_2	L_{13}
Value (mm)	18.5	20	8.5	5.1	6.4	4	16.5	14.6	7	1	7
Parameter	L_4	L_5	L_6	L_7	L_8	L_9	L_{10}	L_{11}	L_{12}	g_3	H
Value (mm)	5.5	3	13	2	7	5.1	28	12.5	7.5	0.8	8.9

2.1. Antenna Evolution Process

The evolution of the proposed dual-band antenna is discussed in this section. Figure 2(a) shows the different stages in the evolution of the proposed dual-band antenna and the corresponding simulated return losses are shown in Figure 2(b). The initial structure (Antenna 1, blue colored) consists of a simple rectangular slot cut in the ground plane. A two stepped signal strip having widths W_{14} and W_{15} and terminated on a hexagonal patch of side length W_{13} is used to capacitively excite the rectangular slot. The feed is slightly asymmetric (shifted towards one side) and has a separation of 0.4 mm with the

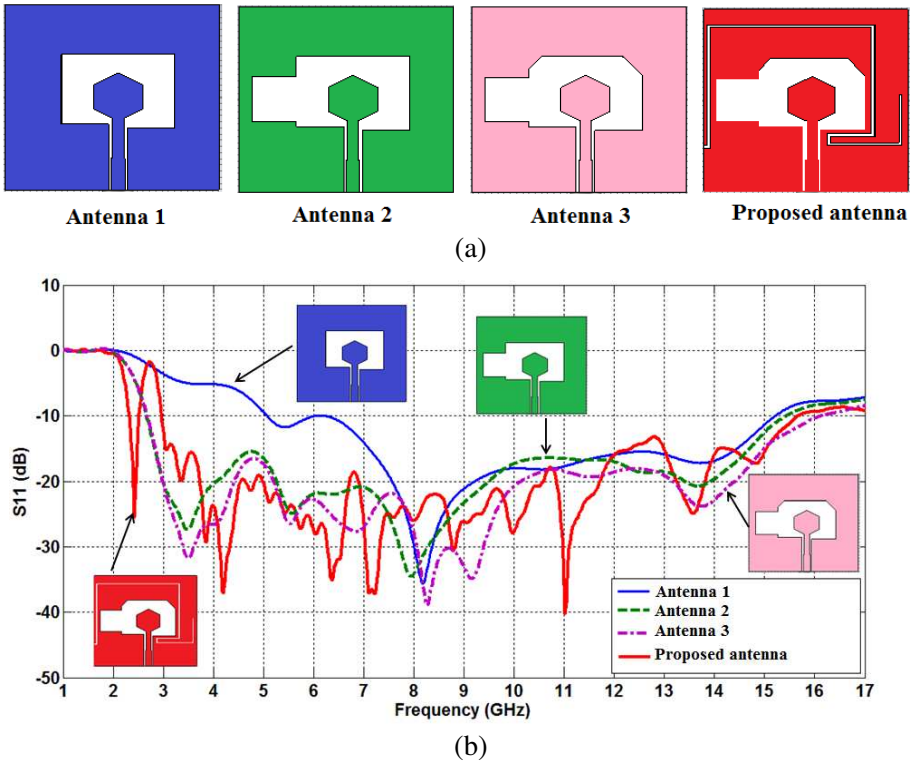

Figure 2. (a) Evolution stages of the proposed dual-band CPW-fed slot antenna. (b) Simulated return loss characteristics for the structures shown in Figure 2(a).

ground plane at the lower end. The two stepped signal strip is used for better impedance matching. The widths are selected such that the feed impedance is near 50 ohms on the connector side and higher than 50 ohms towards the antenna. For efficient excitation and proper impedance matching, the combination of the signal strip and the hexagonal patch should be extended well inside the rectangular slot. The length of the extended combination is denoted as H in Figure 1. This length has a significant effect on the impedance bandwidth of the capacitively coupled slot antenna. With this configuration, an ultra wide impedance bandwidth of 10.0 GHz (from 5.0 to 15.0 GHz) is achieved (Figure 2(b), solid blue line). In order to increase the bandwidth and for better impedance matching at the lower frequency side, an additional rectangular slot in the ground plane is incorporated thereby extending the main slot and making it asymmetric (Antenna 2 and Antenna 3). A large impedance bandwidth of 13.4 GHz (from 2.6 to 16.0 GHz) is achieved by Antenna 3 (Figure 2(b), dashed pink line). This is because the introduction of asymmetric slot in the ground plane creates an extra inductive reactance which neutralizes the capacitive reactance of the initial slot antenna. In the final stage, a slot stub is introduced in the ground plane to generate the extra resonance at 2.4 GHz which can be used for Bluetooth applications (Figure 2(b), solid red line). The shape of the stub is chosen so as to accommodate the length in the available ground plane. The final design (proposed antenna) has impedance bandwidths of 200 MHz from 2.3 to 2.5 GHz and 13 GHz from 3.0 to 16.0 GHz. Thus, the proposed dual-wideband antenna can be used for Bluetooth (2.4–2.484 GHz), WiBro (2.3–2.39 GHz) and UWB applications.

2.2. Role of Asymmetry in Antenna Performance

Two kinds of asymmetries are introduced into the antenna design. In the first asymmetry, the CPW feed line is shifted towards one side which makes the two halves of the ground plane to have unequal dimensions. The second asymmetry is in the slot structure where a rectangular cut is added on one side of the slot. The effect of these asymmetries on the antenna impedance is shown in Figures 3(a) and 3(b) respectively. While the real part of the impedance is plotted in Figure 3(a), the imaginary part

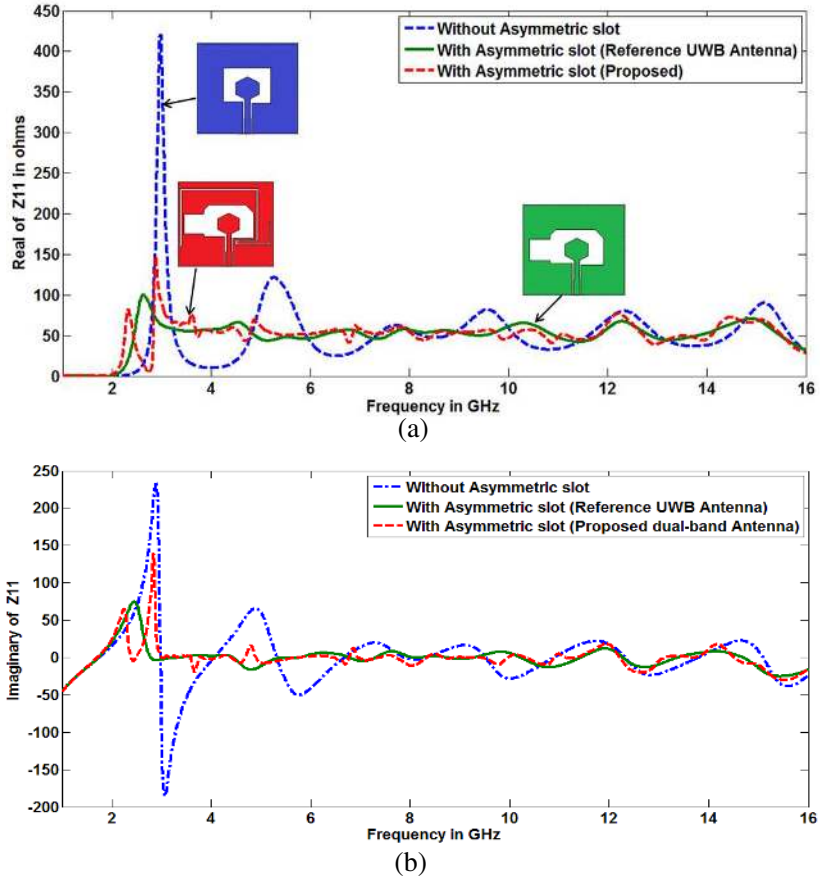

Figure 3. (a) Real part of the input impedance (Z_{11}) of antenna. (b) Imaginary part of the input impedance (Z_{11}) of antenna.

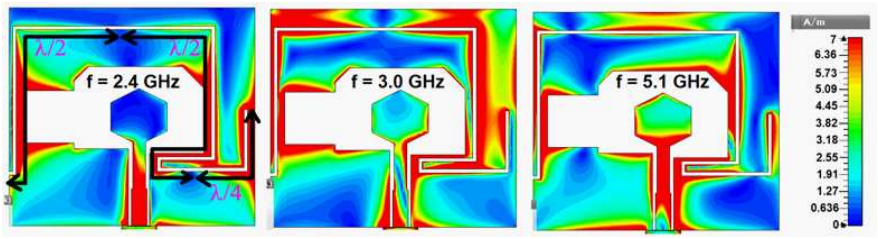

Figure 4. Simulated surface current distributions at 2.4 GHz, 3.0 GHz and 5.1 GHz.

is plotted in Figure 3(b). It is seen from the figures that the introduction of asymmetry reduces the variations in the impedance (both real and imaginary parts) which helps in obtaining better impedance matching over a larger bandwidth. With the asymmetries, the real part gets closer to 50 ohms while the imaginary part gets closer to the 0 ohm line. From a circuit view point, the slot extension (rectangular cut introduced on one side) can be said to introduce an inductance as the reduced metallization to the left of it forces a higher current density. This is also noticed from the current distribution plots discussed later (Figure 4). The inductance so introduced compensates the inherent capacitive reactance offered by a wide slot and brings the imaginary part of the impedance closer to the 0 ohm line. This can be seen specifically in Figure 3(b) near 3 GHz. The improvement in the impedance matching brought about by the feed line asymmetry can be said to be due to the excitation of several new (particularly horizontal) modes in the slot and the ground plane.

2.3. Surface Current Distribution and Expressions for Resonance Frequencies

The antenna surface current distributions at 2.4 GHz, 3.0 GHz and 5.1 GHz are shown in Figure 4. The frequencies selected correspond to some of the resonances seen in the simulated S_{11} curve of the proposed antenna. The red color in the current distribution plot indicates maximum current density while blue color indicates minimum current density. It is known that in case of monopole antennas, both the patch and the ground plane contribute to radiating fields. From Figure 4, it is seen that at 2.4 GHz and 3.0 GHz, the surface current is more on the ground plane and near the narrow slit while little surface current is found on the hexagonal patch. This indicates that the resonance at 2.4 GHz frequency is because of the narrow slit while the resonance at 3.0 GHz is due to the asymmetric rectangular slot. From the figure, it is also observed that at 5.1 GHz, increased current concentration is present on the hexagonal patch. Expression for the first resonance frequency is given in Equation (1). The current distribution around the slit at 2.4 GHz shows a variation of one and one-quarter cycles (in terms of minima and maxima). Hence, at the first resonance, the slit length $L_s = 5\lambda_{eff}/4$. The second resonance frequency in terms of the slot perimeter is given in Equation (2). The third resonance frequency can be approximated by equating the height of the hexagonal patch to $\lambda_{eff}/4$ and it is given by Equation (3).

$$f_1 = \frac{5c}{4L_s\sqrt{\varepsilon}_{r,eff}} \tag{1}$$

$$f_2 = \frac{c}{L_{slot}\sqrt{\varepsilon}_{r,eff}} \tag{2}$$

$$f_3 = \frac{c}{4H\sqrt{\varepsilon}_{r,eff}} \tag{3}$$

$$\varepsilon_{r,eff} = \frac{\varepsilon_r + 1}{2} \tag{4}$$

In the equations, c stands for the velocity of light in free space, $\varepsilon_{r,eff}$ the effective relative permittivity to be calculated from Equation (4), L_s the length of the slit and equal to 96.3 mm, L_{slot} the perimeter of the slot and equal to 66 mm, and H the monopole height equal to 8.9 mm. The values of L_s, L_{slot} and H are obtained from the geometrical details shown in Figure 1 and the parameter values listed in Table 1. For calculating the effective relative permittivity, it is assumed that for a CPW fed monopole, half of the established field lies in air while the remaining half is distributed in the substrate. The calculated resonance frequencies using Equations (1), (2) and (3) are compared against the simulated values in Table 2.

Table 3. Calculated and simulated resonances.

Resonance Frequency	Calculated Value	Simulated Value
f_1	2.37	2.4 GHz
f_2	2.77	3.0 GHz
f_3	5.13	5.1 GHz

3. EXPERIMENTAL AND SIMULATED RESULTS

Based on the optimized parameters given in Table 1, the proposed dual-band antenna was fabricated (Figure 5(a)) on a printed circuit board (PCB) using photolithographic technique. The performance of the antenna was tested using R&S vector network analyzer (ZVA-40). Figure 5(b) shows the measured and CST simulated reflection coefficients of the proposed antenna. From the figure, a good agreement between the measured and simulated results can be seen. The measured impedance bandwidth of the antenna is 200 MHz from 2.3 to 2.5 GHz and 12.1 GHz from 2.9 GHz to 15.0 GHz. It is apparent that the proposed antenna successfully adds an additional band for 2.3 GHz WiBro and 2.4 GHz Bluetooth applications along with ultra wideband performance. The slight difference between the measured and

simulated results is due to uncertainties in the substrate dielectric constant, SMA connector quality, soldering effect and fabrication tolerances.

The far-field radiation patterns and peak gain of the proposed antenna are measured in an in-house anechoic chamber using a standard double ridged horn antenna as the reference. Comparison of the simulated and measured radiation patterns at 2.45 GHz, 3.5 GHz, 5.5 GHz, 6.5 GHz and 8.5 GHz in the E-plane and H-plane are given in Figure 6. It is observed from Figure 6 that in both Bluetooth and UWB bands, the proposed antenna exhibits omnidirectional nature in the H-plane and bi-directional nature in the E-plane. The radiation patterns in the H-plane at middle and higher frequencies (5.5 GHz, 6.5 GHz and 8.5 GHz) are compressed in one direction due to the slot asymmetry and higher order harmonics. For the antenna placed in the co-ordinate system as shown in Figure 1, the H-plane corresponds to

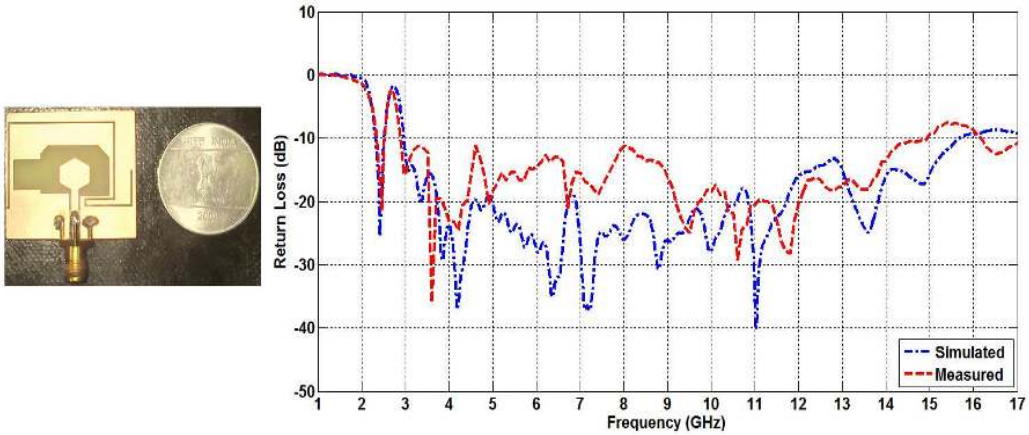

(a) (b)

Figure 5. (a) Fabricated photograph. (b) Measured and simulated reflection coefficient of the proposed dual-band antenna.

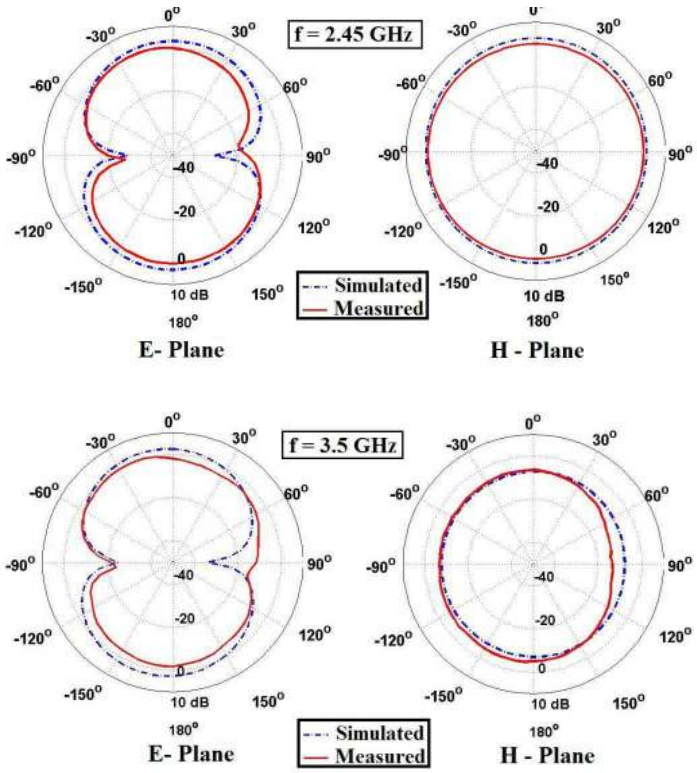

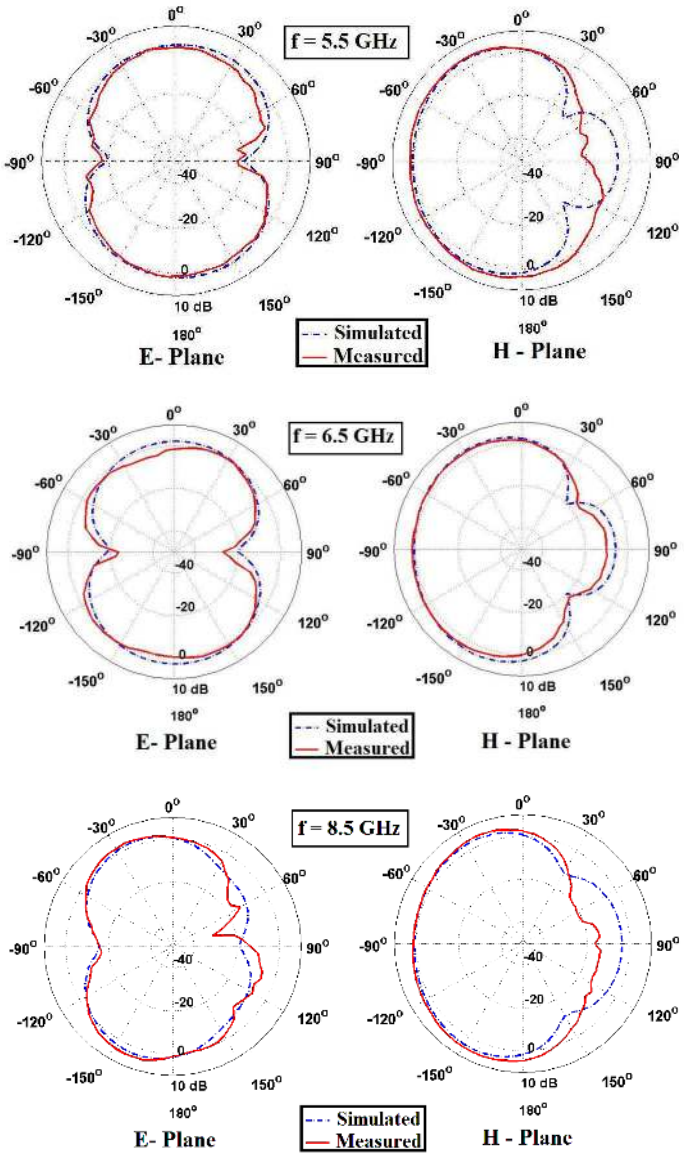

Figure 6. Measured and simulated radiation patterns comparison of the proposed antenna at different resonance frequencies.

the XZ plane while the E-plane corresponds to the YZ plane. As the asymmetry in the antenna is along the XZ plane (slot extension is on the left side) deterioration is seen in the H-plane patterns. At higher frequencies, there is an increase in the current concentration on the reduced ground on the left side which increases the gain along $\theta = -90°$ in comparison to the gain along $\theta = +90°$. In addition to this, the increase in the higher order harmonics also contributes to the deterioration in the radiation patterns to some extent.

Plots of the peak gains (simulated and measured) of the proposed antenna for the bluetooth band and UWB are shown in Figure 7(a) and Figure 7(b), respectively. Again, a good agreement is seen between the measured and simulated gains. While the gain remains between 2–3 dBi in the Bluetooth region, it varies between 3–6 dBi in the ultra wideband. In the ultra wideband region, initially, the gain increases with frequency due to an increase in the effective aperture area at shorter wavelengths. However after around 10 GHz, the gain again becomes less due to an increase in the frequency dependent conductor and substrate losses.

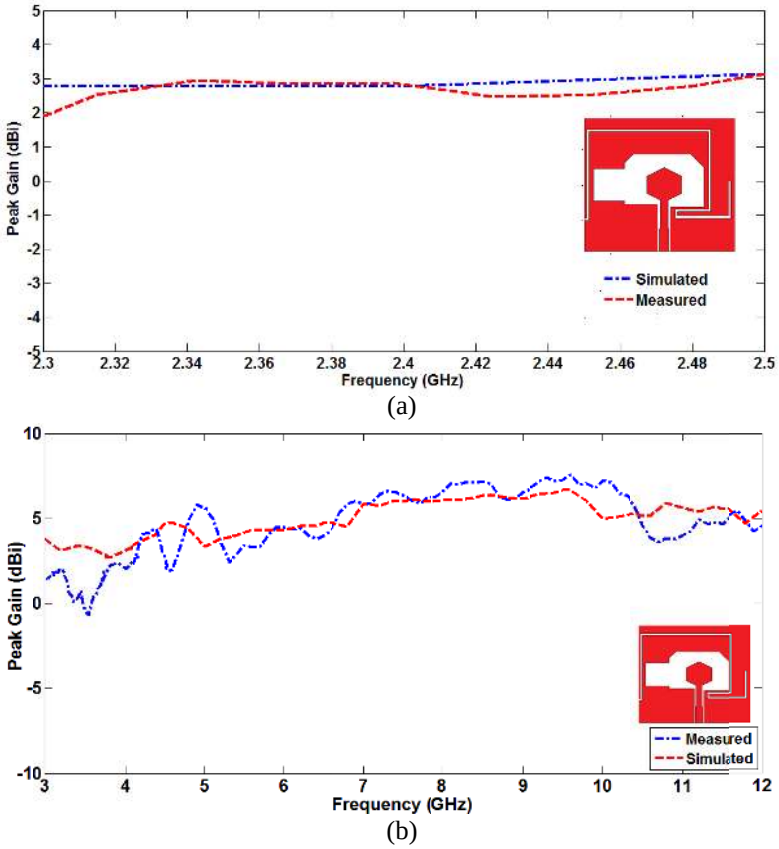

Figure 7. (a) Measured and simulated peak gain comparison of the proposed antenna (First operating band). (b) Measured and simulated peak gain comparison of the proposed antenna (Second operating band).

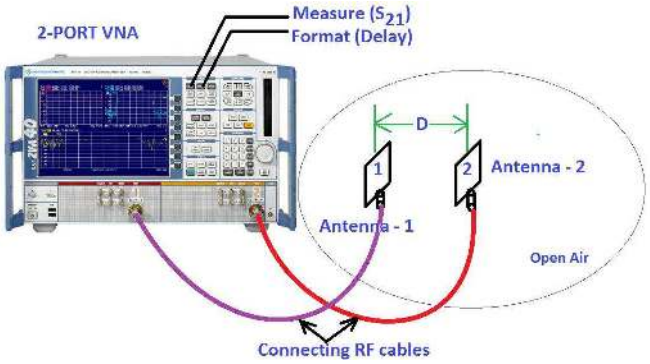

Figure 8. Experimental set up for measuring group delay; Antenna — 1 and Antenna — 2 are identical prototypes of the proposed antenna, $D = 25\,\text{mm}$ (for mutual far field criteria).

4. GROUP DELAY

As the proposed antenna is designed for ultra wideband applications, the time response behavior of the antenna is equally important. A frequency domain performance indicator which indicates a good time response is the group delay. Mathematically, the group delay $\tau(\omega)$ is obtained as the negative derivative of the transmission phase $\phi(\omega)$ with respect to the angular frequency ω.

$$\tau(\omega) = -\frac{d\phi(\omega)}{d\omega} \tag{5}$$

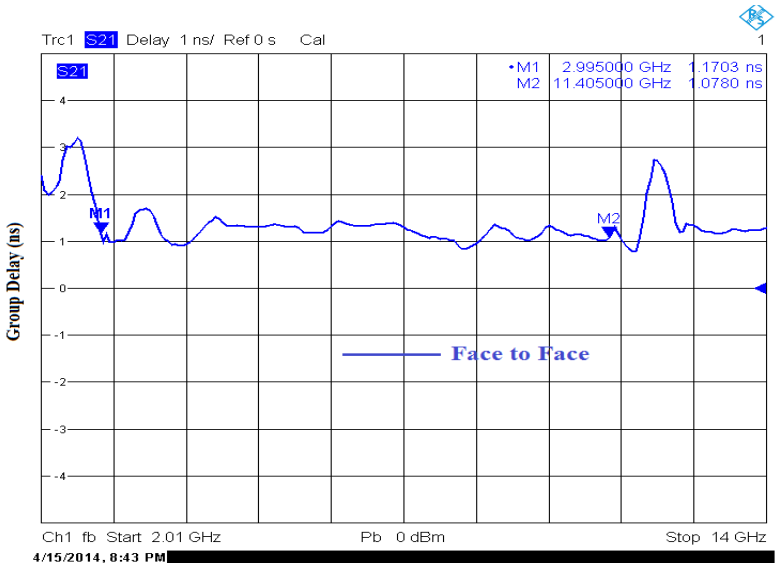

Figure 9. Measured group delay of the proposed antenna in face to face orientation.

To measure the group delay, two identical prototypes of the proposed antenna are fabricated and connected to the two ports of the VNA. The antennas are oriented face to face and placed in the mutual far-field region in an open air environment. The experimental arrangement is shown in Figure 8 while Figure 9 shows the measured group delay. It can be seen from Figure 9 that in the ultra wideband region, the variations in the group delay are less than 1 ns. This indicates phase linearity for the proposed antenna ensuring a faithful reproduction of the transmitted pulse.

5. PARAMETRIC STUDY

The performance of the proposed antenna is decided by various structural parameters. The effects of the key parameters like lengths of the slots (L_s, L_8), widths of the slots (W_s, W_6) and the amount of chamfer as observed through CST simulations are discussed in this section. Figure 10 shows the simulated return loss when the length of the meander slit 'L_s' is varied in case of the proposed dual-band antenna. It is found that the first frequency band is affected by the variation in the 'L_s' while the lower and higher frequency limits of the second (UWB) band remain unchanged. This is due to the fact that the length of the slot 'L_s' determines the first resonant frequency of the dual-band antenna.

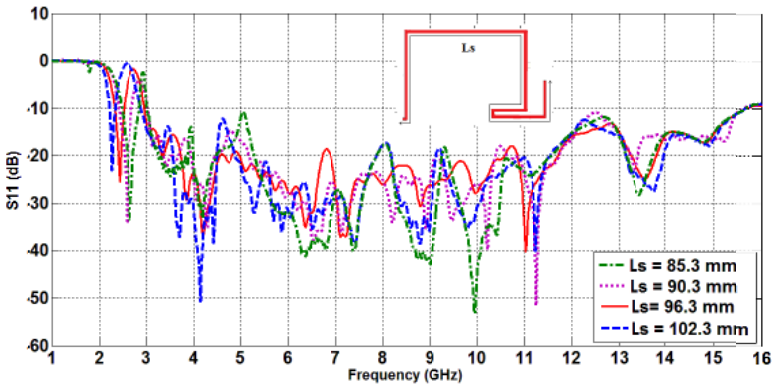

Figure 10. Effect of the narrow rectangular meandered slit length 'L_s' on the return loss of proposed antenna.

In Figure 11, the variations in the simulated return loss when the length of the slot extension 'L_8' is changed are shown. As discussed previously, for the CPW-fed antenna designed, the lower resonance (and cut-off) frequency is decided by the type and size of the slot. Hence, it is seen from Figure 11, that with a change in L_8, the impedance matching over the lower frequencies in the ultra wideband gets severely affected. As L_8 is increased, the impedance matching improves and the lower cut-off frequency reduces. The slot extension however cannot be increased beyond a point due to antenna size constraints. The variations in L_8 are seen to also have a slight effect on the first band (near 2.4 GHz). This is because

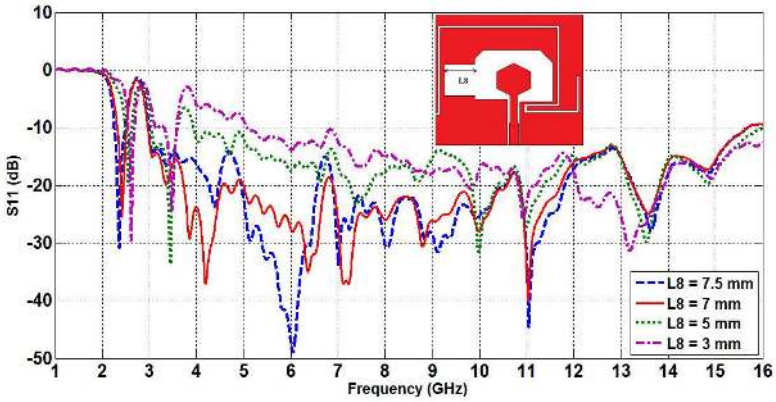

Figure 11. Effect of the slot length 'L_8' on the return loss of proposed antenna.

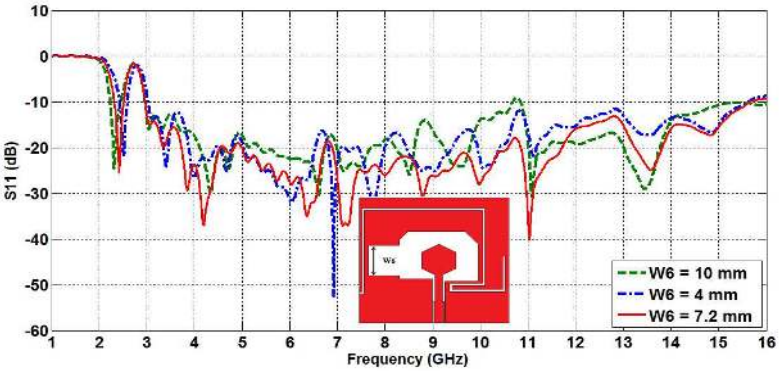

Figure 12. Effect of the slot extension width 'W_6' on the return loss of proposed antenna.

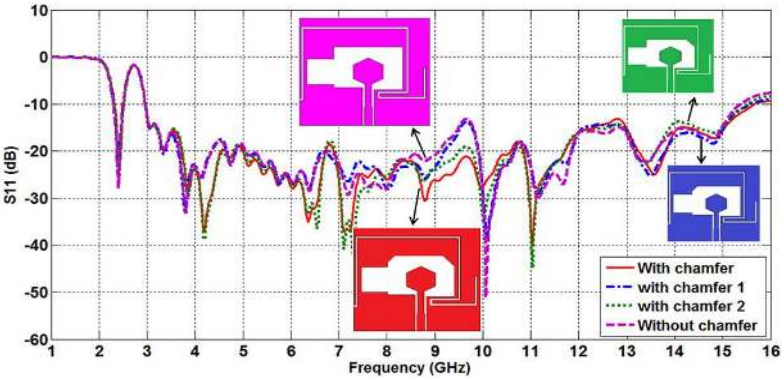

Figure 13. Effect of chamfer on the return loss of proposed antenna.

of increased coupling between the slot and a portion of the narrow rectangular meandered slit as L_8 increases. The increase in L_8 reduces the operating frequency of the first band, implying an increase in the effective length due to coupling. The effect of the width of the slot extension 'W_6' is shown next in Figure 12. As the width increases, the slot perimeter increases and the lower cut-off frequency of the ultra wideband slightly shifts towards the lower end. The impedance matching on the other hand improves over certain frequencies and degrades over the others. This necessitates W_6 to be optimized and the optimal value is found to be 7.2 mm. Similar to the length, the width of the slot extension too has a slight effect on the first operating band. A larger width increases the coupling between the slot and the slit which increases the effective length of the slit and reduces the operating frequency of the first band.

Finally, the effect of the chamfering of the slot corners is shown in Figure 13. In the figure the reflection coefficient characteristics for different cases, i.e., slot without chamfering, slot with one corner chamfered and slot with two corners chamfered are shown. From the figure, it is seen that the slot chamfering at two upper corners provides a correction to the impedance mismatch near 9.7 GHz which brings the S_{11} below -15 dB in the entire ultra wideband.

6. CONCLUSION

A CPW-fed rectangular slot antenna with a hexagonal patch as the radiating element is proposed. Asymmetry is introduced into the antenna design by extending the slot with rectangular cuts placed around it and by shifting the feed line towards one side of the ground plane. The impedance bandwidth obtained with such an arrangement is quite large and covers the FCC UWB requirements. To achieve another narrow band near 2.4 GHz, a narrow meandered rectangular slit is cut in the ground plane. The measured impedance bandwidth of the final design is from 2.3 GHz to 2.5 GHz and from 2.9 GHz to 15.0 GHz. The radiation patterns are measured and found to be omnidirectional in the H-plane and dumb-bell shape in the E-plane. The antenna has a moderate peak gain ranging from 3–7 dBi. The effects of various structural parameters on the antenna performance are shown by means of a parametric study. The antenna will be suitable for Bluetooth, Wireless Broadband (WiBro), medical imaging, ground penetrating radar, vehicular radar and portable UWB wireless applications.

ACKNOWLEDGMENT

The author likes to acknowledge vice-chancellor DIAT (DU), Pune and Symbiosis International University (DU), Pune for continuous support. Author also likes to acknowledge R. V. S. Ram Krishna and Nagendra Kushwaha for their technical suggestions.

REFERENCES

1. "Federal communications commission revision of Part 15 of the Commission's rules regarding ultra-wideband transmission system from 3.1 to 10.6 GHz federal communications commission," 98–153, FCC, Washington, DC, ET-Docket, 2002.
2. Zhao, Q., S.-X. Gong, W. Jiang, B. Yang, and J. Xie, "Compact wide-slot tri-band antenna for WLAN/WiMAX applications," *Progress In Electromagnetics Research Letters*, Vol. 18, 9–18, 2010.
3. Sadat, S., M. Fardis, F. G. Geran, and G. R. Dadashzadeh, "A compact microstrip square-ring slot antenna for UWB applications," *Progress In Electromagnetics Research*, Vol. 67, 173–179, 2007.
4. Azari, A. and J. Rowhani, "Ultra wideband fractal microstrip antenna design," *Progress In Electromagnetics Research C*, Vol. 2, 7–12, 2008.
5. Lee, J. N., J. H. Kim, J. K. Park, and J. S. Kim, "Design of dual-band antenna with U-shaped open stub for WLAN/UWB applications," *Microwave and Optical Technology Letters*, Vol. 51, No. 2, 284–289, Feb. 2009.
6. Zhan, K., Q. Guo, and K. Huang, "A miniature planar antenna for bluetooth and UWB applications," *Journal of Electromagnetic Waves and Applications*, Vol. 24, No. 16, 2299–2308, 2010.

7. Yildirim, B. S., B. A. Cetiner, G. Roquetra, and L. Jofre, "Integrated bluetooth and UWB antenna," *IEEE Antennas Wireless Propag. Lett.*, Vol. 8, 149–152, 2009.
8. Gao, G.-P., "Printed volcano smoke antenna for UWB and WLAN communications," *Progress In Electromagnetics Research Letters*, Vol. 4, 55–61, 2008.
9. Xu, L., B. Yuan, and S. He, "Design of novel UWB slot antenna for bluetooth and UWB applications," *Progress In Electromagnetics Research C*, Vol. 37, 211–221, 2013.
10. Mishra, S. K., R. Gupta, A. Vaidya, and J. Mukherjee, "Printed fork shaped dual band monopole antenna for bluetooth and UWB applications with 5.5 GHz WLAN band notched characteristics," *Progress In Electromagnetics Research C*, Vol. 22, 195–210, 2011.
11. Mishra, S. K., R. K. Gupta, A. Vaidya, and J. Mukherjee, "A compact dual-band fork-shaped monopole antenna for bluetooth and UWB applications," *IEEE Antennas and Wireless Propagation Letters*, Vol. 10, 627–630, 2011.
12. Hung, K.-J. and Y.-C. Lin, "Open-slot loaded monopole antennas for WLAN and UWB applications," *IEEE Antennas and Propagation Society International Symposium 2006*, 4653–4656, Jul. 9–14, 2006.
13. Tao, J., C. H. Cheng, and H. B. Zhu, "Compact dual-band slot-antenna for WLAN applications," *Microwave and Optical Technology Letters*, Vol. 49, No. 5, 1203–1204, 2007.
14. Ren, W., "Compact dual-band slot antenna for 2.4/5 GHz WLAN applications," *Progress In Electromagnetics Research B*, Vol. 8, 319–327, 2008.
15. Wu, J.-W., H.-M. Hsiao, J.-H. Lu, and S.-H, Chang, "Dual broad-band design of rectangular slot antenna for 2.4 and 5 GHz wireless communication," *Electron. Letters*, Vol. 40, 1461–1463, 2004.
16. Xie, J.-J., X.-S. Ren, Y.-Z. Yin, and S.-L. Zuo, "Rhombic slot antenna design with a pair of straight strips and two $\cap$-shaped slots for WLAN/WiMAX applications," *Microwave and Optical Technology Letters*, Vol. 54, No. 6, 1466–1469, 2012.
17. Tsai, L.-C., "A triple-band bow-tie-shaped CPW-fed slot antenna for WLAN applications," *Progress In Electromagnetics Research C*, Vol. 47, 167–171, 2014.
18. Tsai, L.-C., "Design of triple-band T-U-shaped CPW-fed slot antennas," *Microwave and Optical Technology Letters*, Vol. 56, No. 4, 844–848, 2014.
19. Kaur, J. and R. Khanna, "Development of dual-band microstrip patch antenna for WLAN/MIMO/WIMAX/AMSAT/WAVE applications," *Microwave and Optical Technology Letters*, Vol. 56, No. 4, 988–993, 2014.
20. Lin, C. C., E. Z. Yu, and C. Y. Huang, "Dual-band rhombus slot antenna fed by CPW for WLAN applications," *IEEE Antennas and Wireless Propagation Letters*, Vol. 11, 362–364, 2012.